NANO MICRO small

Supporting Information

for *Small,* DOI: 10.1002/smll.202100383

Understanding Carbon Nanotube-Based Ionic Diodes: Design and Mechanism

*Ran Peng, Yueyue Pan, Biwu Liu, Zhi Li, Peng Pan, Shuailong Zhang, Zhen Qin, Aaron R. Wheeler, Xiaowu (Shirley) Tang, and Xinyu Liu**

Supplementary Information (SI) for

Understanding Carbon Nanotube-Based Ionic Diodes: Design and Mechanism

Ran Peng[1,2†], Yueyue Pan[2†], Biwu Liu[3,4], Zhi Li[3], Peng Pan[2], Shuailong Zhang[5,6], Zhen Qin[2], Aaron R. Wheeler[5,6], Xiaowu (Shirley) Tang[3] and Xinyu Liu[2,6]*

[1]*Department of Marine Engineering, Dalian Maritime University, 1 Lingshui Road, Dalian, Liaoning, China 116026*

[2]*Department of Mechanical and Industrial Engineering, University of Toronto, 5 King's College Road, Toronto, Ontario, Canada M5S 3G8*

[3]*Department of Chemistry & Waterloo Institute for Nanotechnology (WIN), University of Waterloo, 200 University Avenue West, Waterloo, Ontario, Canada N2L 3G1*

[4]*Institute of Analytical Chemistry and Instrument for Life Science, The Key Laboratory of Biomedical Information Engineering of Ministry of Education, School of Life Science and Technology, Xi'an Jiaotong University, Xianning West Road, Xi'an, Shaanxi, China 710049*

[5]*Department of Chemistry, University of Toronto, 80 St. George Street, Toronto, Ontario, Canada M5S 3H6*

[6]*Institute of Biomaterials and Biomedical Engineering, University of Toronto, 164 College Street, Toronto, Ontario, Canada M5S 3G9*

*Corresponding author: Xinyu Liu, e-mail: xyliu@mie.utoronto.ca; phone: (+1) 416-946-0558; address: 5 King's College Road, Department of Mechanical and Industrial Engineering, University of Toronto, Toronto, Ontario, Canada M5S 3G8

† Authors contributed equally to this work

Table of contents

SI-1 Parameters applied in the numerical simulation

Table S1 Constants and parameters.

Parameter	Description	Value and unit
$\boldsymbol{\mu}$	Viscosity of electrolyte solution	0.9×10^{-3} [Pa*s]
$\boldsymbol{\rho}$	Density of electrolyte solution	1000 [kg/m^3]
$\boldsymbol{\varepsilon_r}$	Dielectric constant of water	80[1]
$\boldsymbol{\varepsilon_0}$	Permittivity of vacuum	8.854×10^{-12} [F/m]
$\boldsymbol{c_{i\infty}}$	Bulk concentration	1[mol/m^3]
e	Unit charge	1.602×10^{-19} [C]
F	Faraday Constant	9649 [C/mol]
$\boldsymbol{D_1}$	Diffusion coefficient of K^+	1.957×10^{-9} [m^2/s]
$\boldsymbol{D_2}$	Diffusion coefficient of Cl^-	2.032×10^{-9} [m^2/s]
R	Gas constant	8.314[J/mol/K]
$\boldsymbol{k_b}$	Boltzmann constant	1.381×10^{23} [J/K]
T	Temperature	298[K]

SI-2 Fabrication and characterization of the MWCNT-based ionic diode

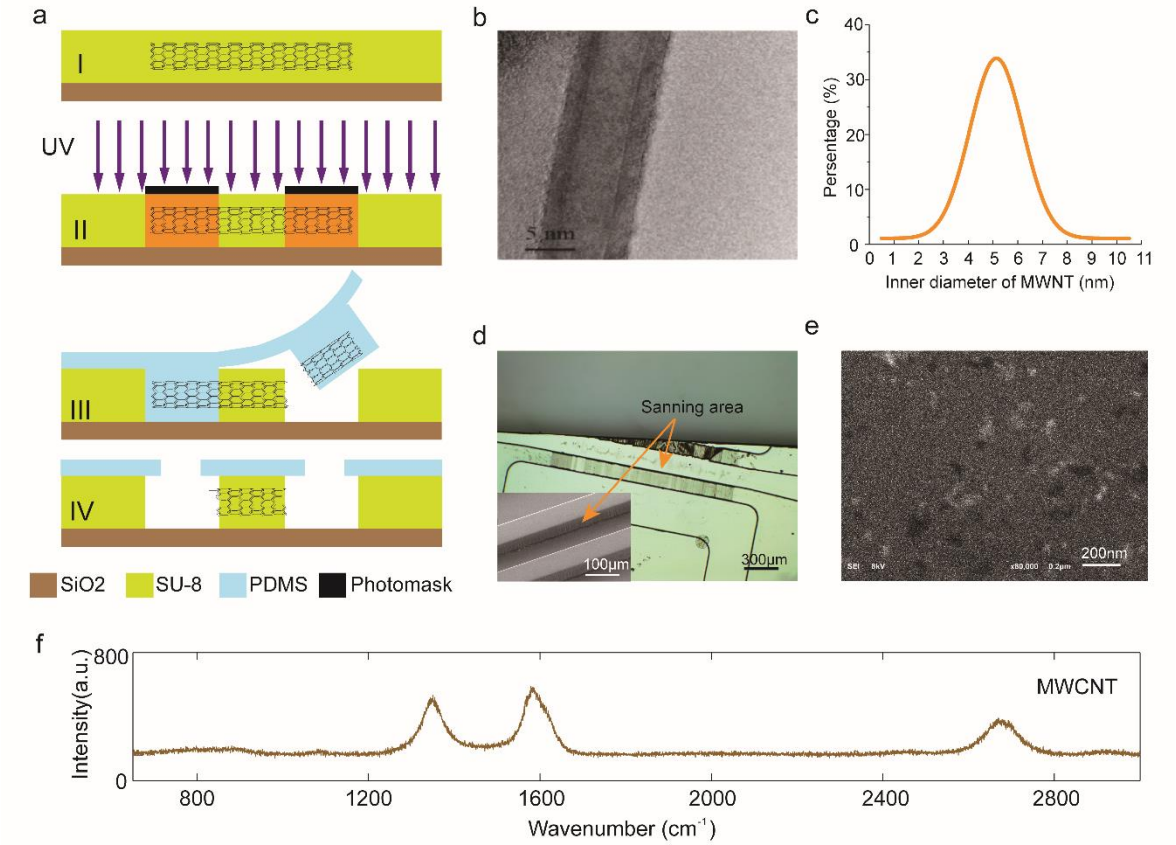

Figure S1 (a) Flow diagram of fabricating CNT nanofluidic chips. (I) Embedding a CNT into a photoresist layer. (II) UV exposure to generate microchannel network. (III) Mechanical avulsion of MWCNT by using PDMS elastomer. (IV) Ready-to-use MWCNT nanofluidic chip after plasma-assisted bonding. (b) TEM image of a MWCNT used for the device fabrication and (c) the inner diameter of the MWCNTs used in this work. (d) Samples for characterizing the MWCNT openings after mechanical avulsion. (e) SEM image of the opening of the MWCNT after mechanical avulsion. (f) Raman shifts of a MWCNT forest.

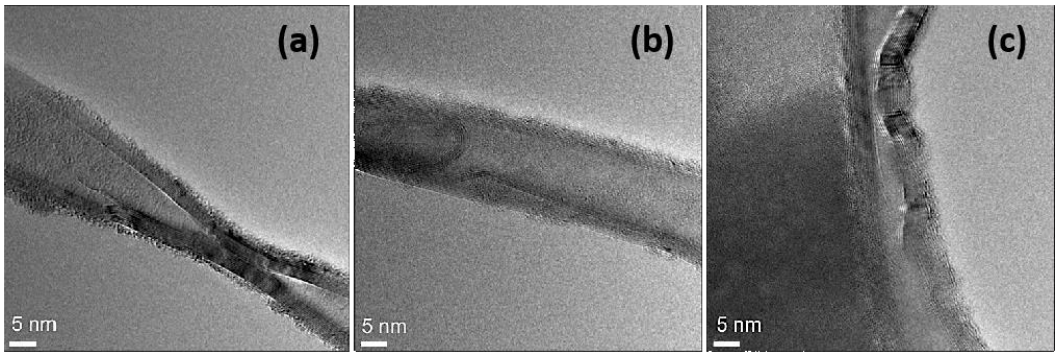

Figure S2 Examples of bamboo-like nodes along the MWCNTs.

SI-3 Summary of ICR performance of selective ionic didoes reported since 2006

Table S2 Summary of ICR ratio of ionic diodes created in recent years specifically based on different nanostructures, conical nanopores, [1–11] nanomembranes [12–24] and nanochannels [25–31] since 2006, in which the nanopore-based ionic diodes are made from polyethylene terephthalate (PET)[1,4,6,8,11], polydimethylsiloxane (PDMS),[2,7] polyimide (PI),[10] silicic solid-state materials,[3,5,9] the nanomembrane-based ionic diodes are developed on hydrogels,[13,19,21] cellulose,[24] graphite oxide (GO),[12,15] combinations of polyelectrolyte-based nanomembranes and nanopores,[14,18,20,22,23] and Janus polyelectrolyte nanomembranes (PENM),[16,17] the nanochannel-based ionic diodes are fabricated by Al_2O_3/SiO_2,[25,26,30] PET[29,31] and CNT.[27,28]

	Materials	Working	Rectification	Year
Conical nanopore/nanochannel	PET	$\pm 5V$	5 [4]	2011
	PET	$\pm 5V$	217 [1]	2006
	PET	$\pm 5V$	300 [11]	2010
	PET	$\pm 0.9V$	65 [6]	2010
	PET	$\pm 2V$	6 [8]	2015
	PDMS	$\pm 1V$	2 [7]	2016
	PDMS/nanoparticles	$\pm 10V$	55 [2]	2007
	Polyimide (PI)	$\pm 2V$	27 [10]	2009
	Silicon nitride (Si3N4)	$\pm 3V$	1.9 [5]	2016
	Silicon	$\pm 3V$	2 [3]	2010
	Borosilicate glass	$\pm 1V$	15 [9]	2019
Nanomembrane	Gel (PDAC/PSS)	$\pm 5V$	40 [13]	2010
	Gel/SiO2	$\pm 5V$	38000 [19]	2018
	Hydrogel PDAC/PSS/CNT composite	$\pm 5V$	9 [21]	2017
	Cellulose	$\pm 5V$	15 [24]	2019
	Porous bock polymer/PET nanopore	$\pm 2V$	1075 [23]	2017
	PIM-EA-TB/PET micropore	$\pm 1V$	180 [20]	2014
	Porous bock polymer/PAA nanopore	$\pm 2V$	489 [22]	2018
	Nafion/PET micropore	$\pm 0.5V$	30 [14]	2017
	Mesoporous carbon/microporous	$\pm 2V$	450 [18]	2016
	Nafion/PIM-EA-TB	$\pm 1V$	64 [17]	2016
	PES-Py/PAEK-HS	$\pm 2V$	57.2 [16]	2015
	SP-GO	$\pm 1V$	48 [12]	2007
	n-Go/p-GO	$\pm 2V$	5.9 [15]	2012
Straight nanochannel	Al2O3/SiO2	$\pm 1V$	300 [26]	2009
	Alumina	$\pm 0.2V$	12 [25]	2009
	Al2O3/SiO2	$\pm 5V$	4.5 [30]	2012
	PET (Dumbbell shaped)	$\pm 2V$	75 [29]	2016
	PET (Conical pore/nanochannel)	$\pm 2V$	553 [31]	2009
	CNT	$\pm 0.5V$	18 [27]	2013
	CNT	$\pm 0.45V$	6 [28]	2018
	CNT	$\pm 5V$	1481.5	This work

SI-4 Numerical simulation results of reservoir size, applied voltage and electroosmotic flow effects on the performance of the MWCNT-based ionic diode

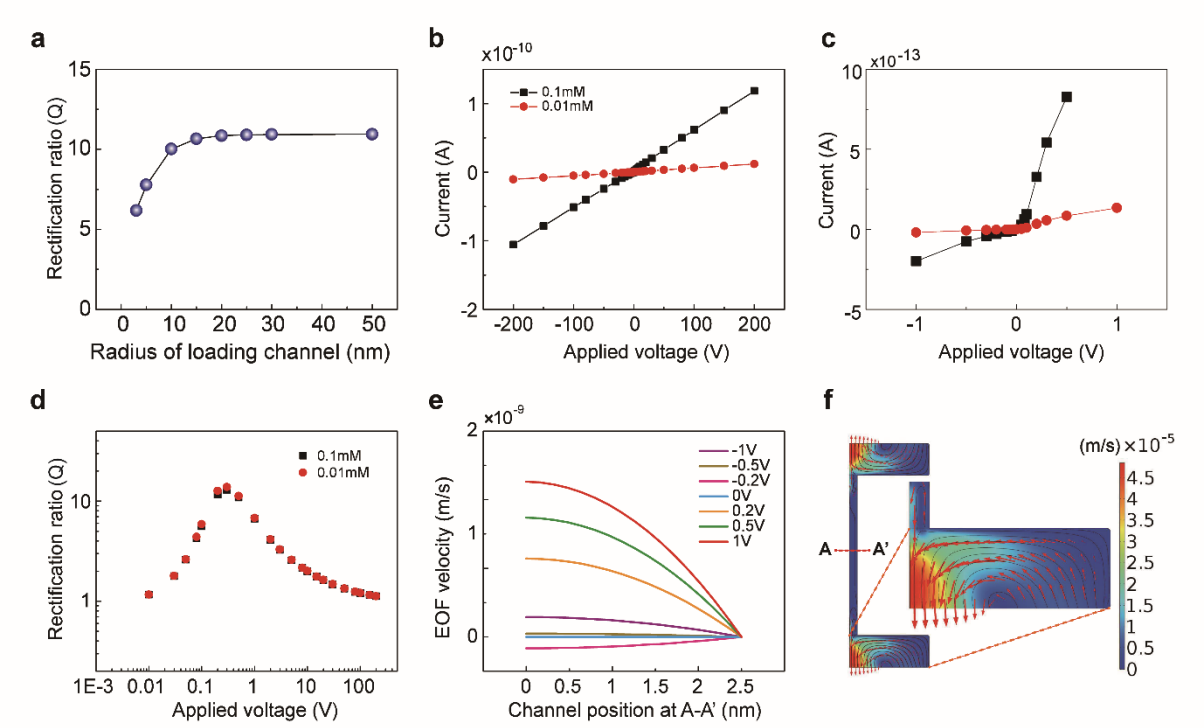

Figure S3 (a) Channel reservoir size effect on the performance of the MWCNT-based ionic diode. The reservoir size affects the ICR performance; however, the effect vanishes when the diameter of the reservoir is larger than 20 nm in radius. In the modelling, the reservoir was 25 nm in radius through this paper. (b) Simulation I-V curves of a MWCNT-based ionic diode working in the range of -200 V to 200 V but with different ionic concentrations of 0.1 mM and 0.01 mM, and (c) a zoomed-in view of the I-V curves working in the range of -1 V to 1 V. (d) Rectification ratio of the I-V curves in (b). (e) Profiles of electroosmotic flow (EOF) velocity at the channel cross-section A-A' marked in (f). (f) Streamlines and arrow-plot of EOF in the nanochannel. In the simulations, a nanochannel of 50 nm long, 5 nm in diameter was applied for all the cases.

SI-5 Numerical simulation results of Debye length and diameter with respect to ICR

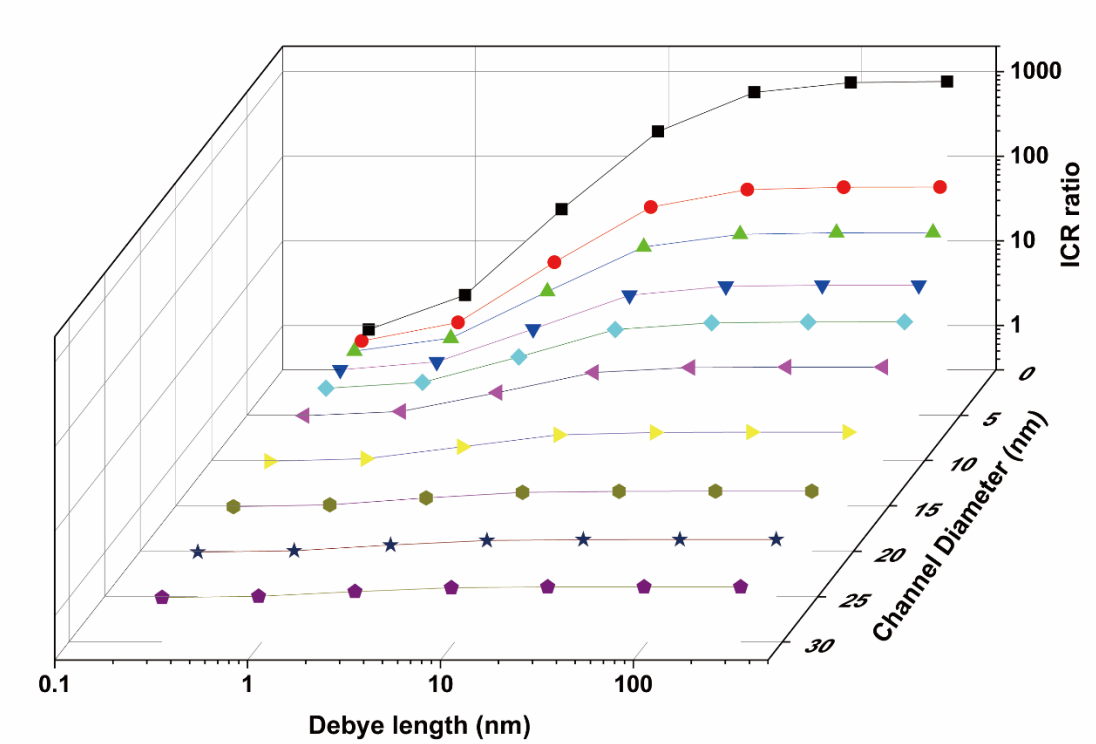

Figure S4 Phase diagram of the Debye length and the channel diameter with respect to the ICR ratio.

SI-6 Numerical simulation results of channel length effects and the charge modification length effects on the performance of the MWCNT-based ionic diode

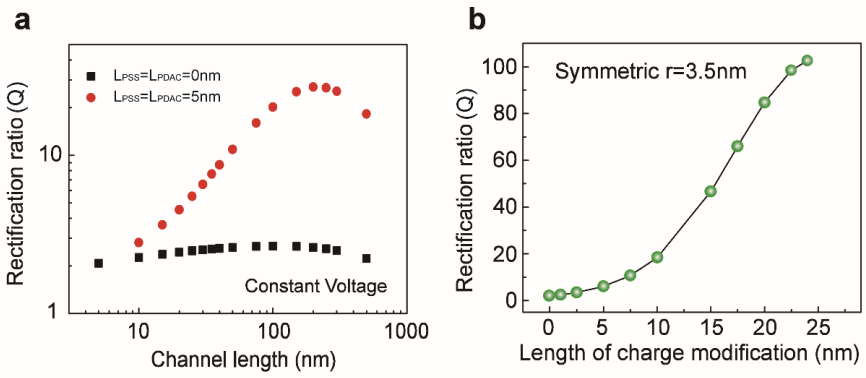

Figure S5 (a) Channel length effects on the ICR performance of the CNT ionic diode working at constant voltages of ±1V. The 50 nm long nanochannel was filled with 0.1 mM KCl solution and modified with 5 nm long charges of ±2 mC^{-2} at the channel terminals. (b) Numerical simulation results of ICR performance of the CNT ionic diode constructed by using a channel of 7 nm in diameter. The numerical model is the same as the one used in the channel length effect study demonstrated in the main text (**Figure 3e**) except for the channel diameter.

SI-7 KCl concentration effects on the performance of the MWCNT-based ionic diode

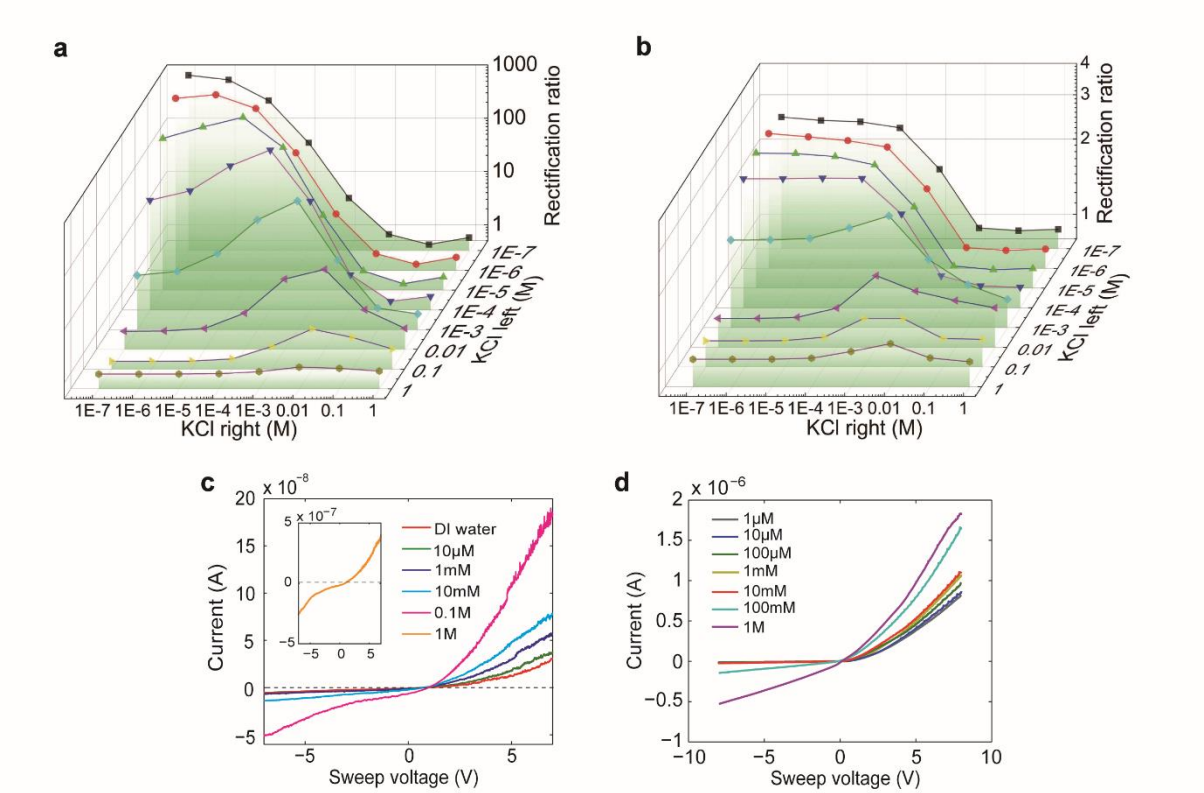

Figure S6 Numerical simulation results of KCl concentration effects on the performance of the MWCNT-based ionic diode of (a) L_{PSS} = L_{PDAC} =24 nm and (b) L_{PSS} = L_{PDAC} = 0 nm modification length. The simulation models are the same as that of the KCl concentration-effect model demonstrated in **Figure 4a** of the main text but with different charge modification lengths. Experimental I-V curves of (c) the symmetric and (d) the asymmetric cases.

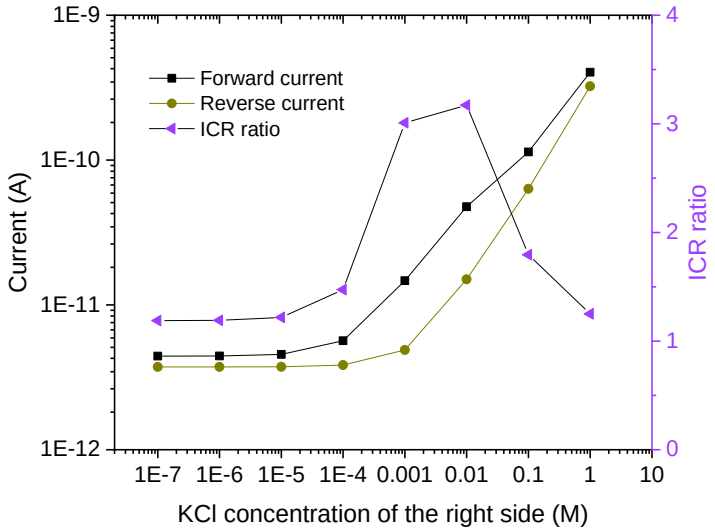

Figure S7 Forward current, reverse current and ICR ratio of the ionic diode working with 10 mM KCl in left side channel and various concentrations of KCl solution in the left side.

SI-8 Charge density/polyelectrolyte concentration effects on the performance of the MWCNT-based ionic diode

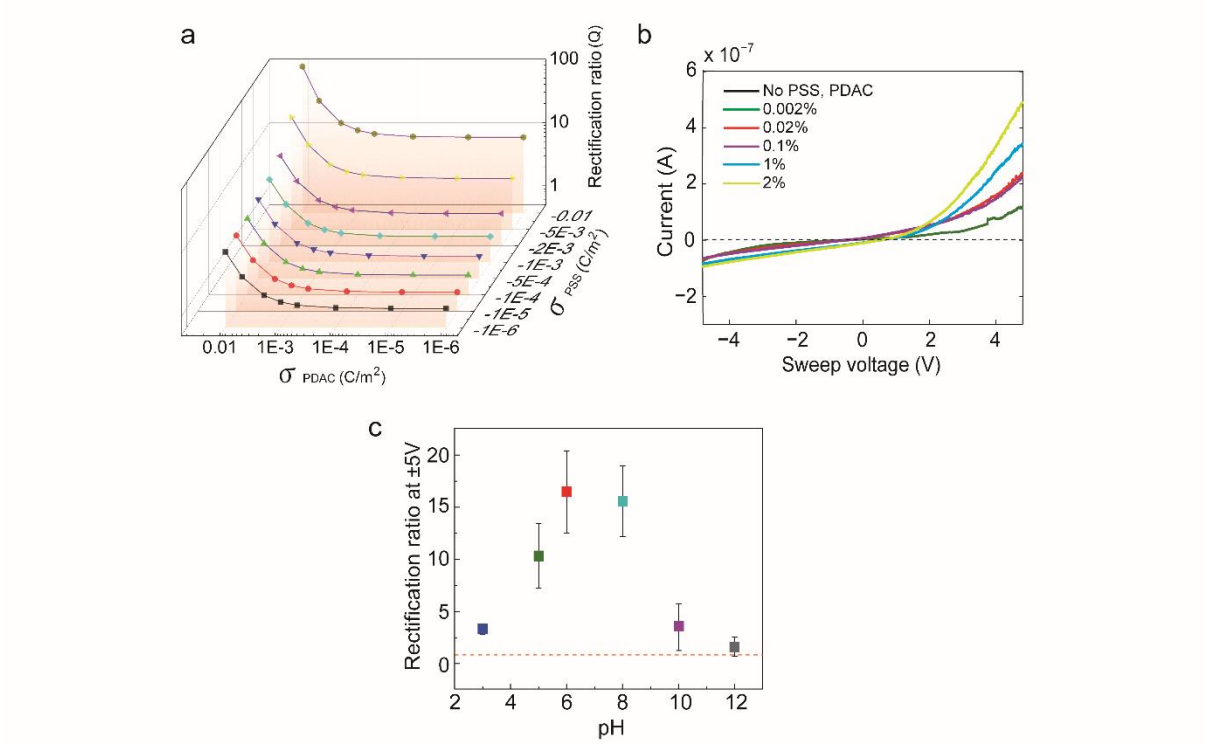

Figure S8 Density of charge modification affects the performance of the MWCNT-based ionic diode. (a) Numerical simulation results of charge density effects on the performance of the ionic diode under the condition of $L_{PSS} = L_{PDAC} = 0$ nm. (b) A family of I-V curves of a MWCNT-based ionic diode working with symmetric concentration of polyelectrolytes (the case of **Figure 5**b). (c) The effects of pH level of the KCl solutions. In the experiments, the microchannels were filled with 1 mM KCl solution containing 1% PDAC or 1% PSS.

References

1 I. Vlassiouk and Z. S. Siwy, *Nano Lett.*, 2007, **7**, 552–556.

2 E. Choi, C. Wang, G. T. Chang and J. Park, *Nano Lett.*, 2016, **16**, 2189–2197.

3 J. Y. Jung, P. Joshi, L. Petrossian, T. J. Thornton and J. D. Posner, *Anal. Chem.*, 2009, **81**, 3128–3133.

4 J. Cervera, B. Schiedt, R. Neumann, S. Mafá and P. Ramírez, *J. Chem. Phys.*, 2006, **124**.

5 Y. Qiu, Z. S. Siwy and M. Wanunu, *Anal. Chem.*, 2019, **91**, 996–1004.

6 L. Wang, Y. Yan, Y. Xie, L. Chen, J. Xue, S. Yan and Y. Wang, *Phys. Chem. Chem. Phys.*, 2011, **13**, 576–581.

7 J. M. Perry, K. Zhou, Z. D. Harms and S. C. Jacobson, *ACS Nano*, 2010, **4**, 3897–902.

8 K. Xiao, P. Li, G. Xie, Z. Zhang, L. Wen and L. Jiang, *RSC Adv.*, 2016, **6**, 55064–55070.

9 E. C. Yusko, R. An and M. Mayer, *ACS Nano*, 2010, **4**, 477–487.

10 G. Xie, K. Xiao, Z. Zhang, X. Y. Kong, Q. Liu, P. Li, L. Wen and L. Jiang, *Angew. Chemie - Int. Ed.*, 2015, **54**, 13664–13668.

11 G. Nguyen, I. Vlassiouk and Z. S. Siwy, *Nanotechnology*, 2010, **21**.

12 L. Wang, Y. Feng, Y. Zhou, M. Jia, G. Wang, W. Guo and L. Jiang, *Chem. Sci.*, 2017,

8, 4381–4386.
13 O. J. Cayre, T. C. Suk and O. D. Velev, *J. Am. Chem. Soc.*, 2007, **129**, 10801–10806.
14 K. Mathwig, B. D. B. Aaronson and F. Marken, *ChemElectroChem*, 2018, **5**, 897–901.
15 X. Zhang, Q. Wen, L. Wang, L. Ding, J. Yang, D. Ji, Y. Zhang, L. Jiang and W. Guo, *ACS Nano*, 2019, **13**, 4238–4245.
16 X. Zhu, J. Hao, B. Bao, Y. Zhou, H. Zhang, J. Pang, Z. Jiang and L. Jiang, *Sci. Adv.*, 2018, **4**, 1–9.
17 B. Riza Putra, M. Carta, R. Malpass-Evans, N. B. McKeown and F. Marken, *Electrochim. Acta*, 2017, **258**, 807–813.
18 J. Gao, W. Guo, D. Feng, H. Wang, D. Zhao and L. Jiang, *J. Am. Chem. Soc.*, 2014, **136**, 12265–12272.
19 H. J. Koo, S. T. Chang and O. D. Velev, *Small*, 2010, **6**, 1393–1397.
20 Y. Rong, Q. Song, K. Mathwig, E. Madrid, D. He, R. G. Niemann, P. J. Cameron, S. E. C. Dale, S. Bending, M. Carta, R. Malpass-Evans, N. B. McKeown and F. Marken, *Electrochem. commun.*, 2016, **69**, 41–45.
21 Y. Zhou, Y. Hou, Q. Li, L. Yang, Y. Cao, K. H. Choi, Q. Wang and Q. M. Zhang, *Adv. Mater. Technol.*, 2017, **2**, 1–6.
22 Z. Zhang, X. Y. Kong, K. Xiao, G. Xie, Q. Liu, Y. Tian, H. Zhang, J. Ma, L. Wen and L. Jiang, *Adv. Mater.*, 2016, **28**, 144–150.
23 Z. Zhang, X. Y. Kong, K. Xiao, Q. Liu, G. Xie, P. Li, J. Ma, Y. Tian, L. Wen and L. Jiang, *J. Am. Chem. Soc.*, 2015, **137**, 14765–14772.
24 W. Zhang, X. Zhang, C. Lu, Y. Wang and Y. Deng, *J. Phys. Chem. C*, 2012, **116**, 9227–9234.
25 Y. Kong, X. Fan, M. Zhang, X. Hou, Z. Liu, J. Zhai and L. Jiang, *ACS Appl. Mater. Interfaces*, 2013, **5**, 7931–7936.
26 L. J. Cheng and L. J. Guo, *ACS Nano*, 2009, **3**, 575–584.
27 J. Wu, X. Zhan and B. J. Hinds, *Chem. Commun.*, 2012, **48**, 7979–7981.
28 N. R. Scruggs, J. W. F. Robertson, J. J. Kasianowicz and K. B. Migler, *Nano Lett.*, 2009, **9**, 3853–3859.
29 K. Xiao, L. Chen, G. Xie, P. Li, X. Y. Kong, L. Wen and L. Jiang, *Nanoscale*, 2018, **10**, 6850–6854.
30 R. Yan, W. Liang, R. Fan and P. Yang, *Nano Lett.*, 2009, **9**, 3820–3825.
31 K. Xiao, G. Xie, Z. Zhang, X. Y. Kong, Q. Liu, P. Li, L. Wen and L. Jiang, *Adv. Mater.*, 2016, **28**, 3345–3350.